Realistic shell-model calculations and exotic nuclei

A. Gargano[a], L. Coraggio[a], A. Covello[a,b], N. Itaco[a,b]
[a] *Istituto Nazionale di Fisica Nucleare, Complesso Universitario di Monte S. Angelo, I-80126 Napoli*
[b] *Dipartimento di Fisica, Università di Napoli Federico II, Complesso Universitario di Monte S. Angelo, I-80126 Napoli*
(Dated: March 12, 2014)

This paper presents a short overview of the shell-model approach with realistic effective interactions to the study of exotic nuclei. We first give a sketch of the current state of the art of the theoretical framework of this approach, focusing on the main ingredients and most relevant recent advances. Then, we present some selected results for neutron-rich nuclei in various mass regions, namely oxygen isotopes, $N = 40$ isotones, and nuclei around ^{132}Sn, to show the merit as well as the limits of these calculations.

arXiv:1403.2398v1 [nucl-th] 10 Mar 2014

I. INTRODUCTION

The shell model has long proved to be a main key to the understanding of nuclear structure. It provides the theoretical framework for a microscopic description of nuclear properties which is essentially based on the use of effective interactions. In fact, as is well known, within the shell-model approach only the particles outside a core made up of filled shells (valence particles) are considered to be active, and calculations are performed in a truncated Hilbert space, the so-called model space. The shell-model Hamiltonian acting only between the valence particles should, therefore, account for the neglected degrees of freedom, namely those of the core particles as well as of the excitations of valence particles above the chosen model space.

To this end, one can resort to empirical interactions, *i.e.* interactions containing adjustable parameters or obtained by treating the matrix elements themselves as free parameters. In both cases fitting procedures to reproduce the experimental data are required. Empirical interactions have been used in a number of shell-model calculations, providing in most cases a successful description of a variety of nuclear phenomena.

Clearly, a more fundamental approach to the shell model consists in starting from the interaction between free nucleons and constructing the Hamiltonian by means of many-body techniques, which leads to what is called "realistic effective interaction". This alternative way, based on a microscopic derivation of the shell-model effective interaction, has the great advantage that no adjustable parameter is needed and establishes a bridge between effective shell-model interactions and underlying nuclear forces. Significant progresses have been made along this line in the last two decades, and realistic shell-model calculations have been shown to provide an accurate description of nuclear structure properties for nuclei in various mass region both close to and far from the stability valley.

In this context, it should be mentioned that in many shell-model calculations, in particular those aiming at interpreting the new experimental data obtained at Radioactive Ion Beam (RIB) facilities, use has also been made of semi-empirical interactions, consisting in modified versions of realistic effective interactions. Here, however, we focus only on shell-model calculations employing genuine realistic effective interactions and give a brief description of the current status of this approach. We firstly review the main steps and the relevant recent developments involved in the perturbative technique used to derive the shell-model interaction from the bare nuclear potential. Then, we report some results we have obtained for various neutron-rich nuclei, as oxygen isotopes [1, 2], $N = 40$ isotones [3], and nuclei around ^{132}Sn [4], to show the practical value of this approach as well as its limits.

The basic ingredient of realistic shell-model calculations is the bare nuclear potential, for which, as is well known, there are various reliable models. However, we shall not discuss this point here. In the calculations concerned with the present contribution we have used two modern nucleon-nucleon (NN) potentials, the CD-Bonn [5] and N^{3}LOW potential [1], which fit equally well the NN scattering data. In particular, the calculations for $N = 40$ isotones and nuclei around ^{132}Sn have been performed with the former while results for oxygen isotopes have been obtained with the latter. It is worth recalling that, owing to its strong short-range repulsive behavior, the CD-Bonn potential cannot be used directly in deriving the effective interaction within the framework of a perturbative approach. In other words, it must be first renormalized, which is done by constructing a low-momentum potential $V_{\mathrm{low-k}}$ defined within a cutoff momentum Λ [6]. This is a smooth potential which preserves exactly the onshell properties of the original one. As concerns the N^{3}LOW potential, this is derived from the chiral perturbation theory with a sharp momentum cutoff at 2.1 fm^{-1} . It is conceived therefore as a low-momentum potential and no renormalization procedure is needed.

Finally, we would like to point out that our effective interactions are all based only on bare NN potentials, namely three-body forces are not explicitly considered. The study of the role of three body forces in nuclear structure has recently attracted great theoretical interest. Their effects have been evidenced within the framework

of *ab initio* approaches for few nucleon systems. Until now, however, no shell-model calculation has been performed with an effective Hamiltonian derived by treating on equal footing both NN and $3N$ forces. This, which would imply the appearance of further core-polarization effects on the one- and two-body components as well as of an effective three-body term, is quite a complex project. Actually, only first-order contributions of the normal-ordered one- and two-body parts of $3N$ forces have been taken explicitly into account. In connection with the role of 3N forces, however, it should be mentioned that in a recent paper [7] an optimized NN interaction derived from the chiral effective field theory has been constructed, which seems to account for many aspects of nuclear structure without explicitly including $3N$ forces.

II. THEORETICAL FRAMEWORK

Let us start with the Schrödinger equation for a system of A nucleons interacting via two-body forces

$$H\Psi_\alpha = E_\alpha \Psi_\alpha, \tag{1}$$

where

$$H = T + V_{\rm NN}, \tag{2}$$

T being the kinetic energy and $V_{\rm NN}$ a low-momentum two-body potential, obtained through the $V_{\rm low-k}$ procedure [6] or purposely constructed to have a smooth perturbative behavior, with the addition of the Coulomb force for protons.

Now, by introducing an auxiliary one-body potential U the Hamiltonian (2) can be written as

$$H = (T+U) + (V_{NN} - U) = H_0 + H_1, \tag{3}$$

namely as a one-body component H_0, which describes the independent motion of the nucleons, and a residual interaction H_1.

The effective Hamiltonian, $H_{\rm eff}$, is defined through the model-space eigenvalue problem

$$H_{\rm eff} P|\Psi_\alpha\rangle = H_0 P|\Psi_\alpha\rangle + H_1^{\rm eff} P|\Psi_\alpha\rangle = E_\alpha P\Psi_\alpha, \tag{4}$$

where the E_α and the corresponding Ψ_α are a subset of the eigenvalues and eigenfunctions of the original Hamiltonian. Clearly, $H_{\rm eff}$ acts only on the model space defined in terms of the eigenvalues of H_0 through the projection operator P.

A well-established approach to the determination of the effective Hamiltonian is given by the $\hat{Q}$-box folded-diagram expansion. A detailed description of this approach can be found in Refs. [8, 9], so we will not touch upon it here. We would like, however, to highlight the main points involved in the derivation of $H_{\rm eff}$, so as to make clear the present stage of development.

Within a degenerate model space, $PH_0P = \epsilon_0$, iterative techniques [10] can be used to construct the effective Hamiltonian. These, as the Krenciglowa-Kuo (KK) and the Lee-Suzuki (LS) ones, are based on an expansion of $H_1^{\rm eff}$ in terms of the $\hat{Q}$-box and its derivatives, the $\hat{Q}$-box being defined as

$$\hat{Q}(\epsilon) = PH_1P + PH_1Q\frac{1}{\epsilon - QHQ}QH_1P, \tag{5}$$

where the operator Q is the complement of P.

Once the $\hat{Q}$-box is calculated, we derive $H_1^{\rm eff}$ by means of the LS technique, which yields converged results after a small number of iterations. The calculation of the $\hat{Q}$-box, however, is the most critical step of our procedure. This is performed by writing the term $1/(\epsilon - QHQ)$ in equation (5) as a power series, which leads to a perturbative calculation to be performed under some approximations. A diagrammatic representation of the $\hat{Q}$-box, including one- and two-body diagrams up to third order in the interaction, is given in Ref. [9]. Clearly, only diagrams up to a finite order can be included and the state-of-the-art calculations do not go beyond the third order. One should also consider that the evaluation of the diagrams composing the $\hat{Q}$-box requires, in principle, a summation over all the states of the Q space. The truncation of this infinite space is, therefore, another source of approximation. Both the order-by-order and the intermediate-state convergence of the effective interaction expansion are briefly reviewed in [8, 11] where references to previous works are given, while in [9] they are discussed in detail focusing on p-shell nuclei. In section 3, results of shell-model calculations with effective interactions derived by including diagrams up to second as well as third order are reported and compared with experimental data.

In concluding this outline of the theoretical framework, it is worth mentioning two other points entering our procedure. Our effective Hamiltonian is derived for a two-valence-particle nucleus but is then used for systems with a larger number of valence particles. This means that we only include one- and two-body forces neglecting higher-body terms, which arise as an effect of the nuclear medium even if an NN potential is used. The one-body force gives the theoretical single-particle energies as resulting from the sum of the eigenvalues of H_0 and the one-body contributions of $H_1^{\rm eff}$. In most realistic shell-model calculations, however, these energies are replaced by values taken from experiment. Furthermore, we note that the perturbation expansion is performed for $H_1 = V_{\rm NN} - U$, which gives rise to $(V-U)$-insertion diagrams (see [9]), which are in general neglected with the exception of the first-order ones. As a matter of fact, these are exactly zero only when taking for U a self-consistent Hartree-Fock potential, whereas an harmonic oscillator potential is generally used. In the next section we shall present results obtained by using both theoret-

ical and experimental single-particle energies as well as by including or not $(V-U)$-insertion diagrams beyond the first order.

III. RESULTS FOR VARIOUS MASS REGIONS

We discuss and compare with experiment results for O isotopes, $N=40$ isotones, and ^{132}Sn neighboring nuclei, which have been obtained within the shell-model framework using realistic effective interactions. Most of the results presented in this section have already been given in previous works [2–4], but our aim here is to give a panoramic view of them in order to show the ability of these effective interactions to describe neutron-rich nuclei in different mass regions.

A. Oxygen isotopes

One of the challenging problems in modern nuclear structure studies concerns the location of the neutron drip line, namely the limit of existence of neutron-rich systems. In this context, the oxygen isotopes play an important role. The drip line for $Z=8$ is quite close to the stability valley, in contrast with the situation that occurs for other isotopes in the same mass region. As a matter of fact, the limit for oxygen isotopes is established at $N=16$, the last stable one being ^{18}O. Several calculations [12–14] have been recently performed suggesting that the explanation for this limit resides in $3N$ forces.

The effective Hamiltonian for oxygen isotopes is derived for the *sd* space with ^{16}O as inert core starting from the N^3LOW potential with a sharp cutoff at 2.1 fm^{-1}, which is a low-momentum realistic NN interaction derived from the chiral perturbation theory. All diagrams up to third order are taken into account in the calculation of the $\hat{Q}$-box including the $(V-U)$-insertion diagrams. As regards the energies of the three single-particle orbitals of the *sd* space, we employ the theoretical values, as arising from the one-body contributions of $H_{\rm eff}$.

In figure 1, the calculated excitation energies of the yrast 2^+ states are compared with the experimental values [15]. We see that our predictions are in very good agreement with the observed energies. In particular, we reproduce the rise from $A=20$ to 22 as well as that from $A=22$ to 24 which are related to the $N=14$ and 16 subshell closure, respectively.

To test the ability of our interaction to reproduce the location of the drip line for oxygen isotopes, we have calculated the ground-state (g.s.) energies, which are compared in figure 2 with the experimental values [16]. The theoretical curve lies below the experimental one, with a discrepancy increasing with the number of neutrons. Actually, our calculations overestimate the experimental g.s. energies and fail to predict ^{26}O and ^{28}O as unbound nuclei. In the same figure, however, we show the results

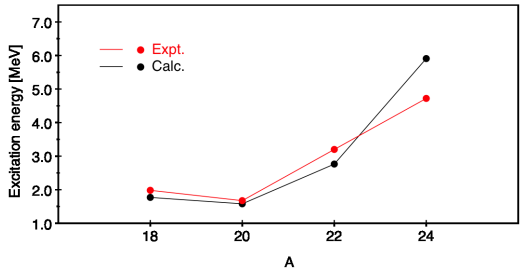

FIG. 1: (Color online) Excitation energies of yrast 2^+ states in O isotopes from $A=18$ to 24 .

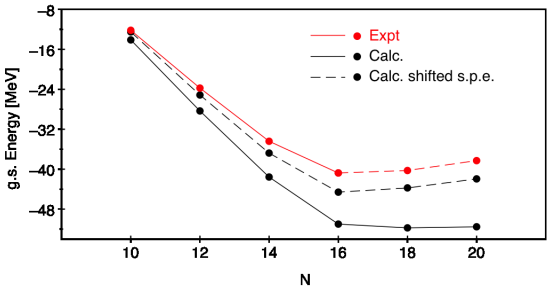

FIG. 2: (Color online) Ground-state energies for O isotopes from $N=10$ to 20 (see text for details).

that are obtained by an upshift (427 keV) of the calculated single-particle spectrum so as to reproduce the experimental g.s. energy of ^{17}O relative to ^{16}O. The new curve moves up coming closer to the experimental one and shows the right slope from $N=16$ on. This highlight some inaccuracy in our one-body effective Hamiltonian which may be traced to the lack of three-body forces.

B. $N=40$ isotones

We now present and discuss our results for the $N=40$ isotones Ca, Ti, Cr, Fe, and Ni. Before doing so, however, a few comments are in order. The experimental behavior of the excitation energy of the 2^+ yrast state in Ni isotopes, and in particular the sizable increase in ^{68}Ni with respect to the two neighboring even isotopes, evidences a subshell closure at N=40. For a decreasing number of protons this closure disappears and the onset of a collective behavior is observed. This issue is currently the subject of great experimental and theoretical interest (see [17–20] and references therein), and the appearance of the collective behavior has been traced to the correlations between the quadrupole-partner neutron orbitals $0g_{9/2}$ and $1d_{5/2}$ [17].

With the aim of directly testing the role played by the neutron $1d_{5/2}$ orbital, we have performed realistic shell-model calculations taking ^{48}Ca as inert core and

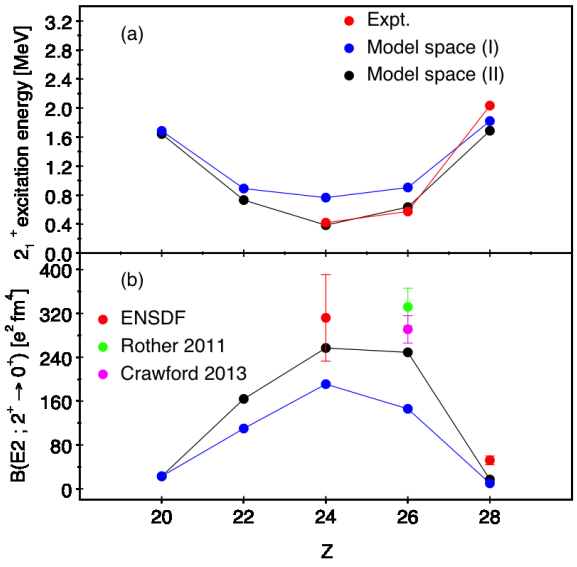

FIG. 3: (Color online) (a) Experimental (ENSDF [15], Rother [18], Crawford [20]) and calculated excitation energies of the yrast 2^+ states and (b) $B(E2; 2_1^+ \rightarrow 0_1^+)$ for the $N = 40$ isotones.

considering two different model spaces. The first one, model space (I), is spanned by the proton $0f_{7/2}$ and $1p_{3/2}$ orbitals and by the neutron $1p_{3/2}$, $1p_{1/2}$, $0f_{5/2}$, $0g_{9/2}$ orbitals while the second one, model space (II), includes the same orbitals with the addition of the neutron $1d_{5/2}$ one. We calculate the effective interaction starting from the CD-Bonn NN potential renormalized by way of the $V_{\rm low-k}$ approach with a cutoff momentum $\Lambda = 2.6$ fm^{-1}. As for the O isotopes, all diagrams up to third order are taken into account in the calculation of the $\hat{Q}$-box, but at variance with the previous case the single-particle energies are determined using experimental data. More details on our effective Hamiltonian, including the values of the single-particle energies and a list of the two-body matrix elements in the model spaces (I) and (II) are given in Ref. [3].

In figure 3, we report the excitation energies of the yrast 2^+ states and the $B(E2; 2_1^+ \rightarrow 0_1^+)$ transition rates for the $N = 40$ isotones as a function of Z. As regards the energies, we see that both calculated curves reproduce well the observed behavior, but the inclusion of the neutron $1d_{5/2}$ orbital is essential for a quantitative agreement with the experimental data. The role of this orbital appears even more relevant when looking at the $B(E2)$ transition rates. Only the $B(E2)$'s for ^{64}Cr, ^{66}Fe, and ^{68}Ni are experimentally known, and these values for the former two nuclei are significantly underestimated by our calculations with model space (I), while this is not the case when model space (II) is used. Our results, therefore, confirm the connection between the $1d_{5/2}$ orbital and the appearance of collectivity in Ti, Cr, and Fe, as evidenced by the lowering of the 2_1^+ state and the increase in the corresponding $B(E2)$. To better understand this point, we show in table I the occupation numbers of the proton $\pi f_{7/2}$ and neutron $\nu g_{9/2}$ and $\nu d_{5/2}$ orbitals for the ground state of Ti, Cr, Fe, and Ni.

TABLE I: Occupation numbers of the proton $\pi f_{7/2}$ and neutron $\nu g_{9/2}$ and $\nu d_{5/2}$ orbitals for the ground state of the $N = 40$ isotones (see text for details).

		Ti	Cr	Fe	Ni
$\pi f_{7/2}$	(I)	1.87	3.64	5.61	7.89
	(II)	1.69	3.31	5.31	7.85
$\nu g_{9/2}$	(I)	3.23	2.88	1.75	0.42
	(II)	3.72	3.73	2.81	0.47
$\nu d_{5/2}$	(II)	0.36	0.57	0.33	0.05

We see that there are no substantial differences between the occupation numbers obtained with model spaces (I) and (II) for Ni. In both cases, a very low occupancy of protons (0.11-0.15) is found above the $0f_{7/2}$ orbital as well as of neutrons (0.42-0.52) above the $0f_{5/2}$ orbital, the latter result implying a clear manifestation of subshell closure at $N = 40$. Note that, with model space (II), only 0.05 neutrons occupy the $1d_{5/2}$ orbital which gives reason for its minor role in the description of ^{68}Ni. However, when decreasing the number of protons the two model spaces lead to significantly different results. In fact, when going from model space (I) to model space (II) we find an increase in the occupation number of the neutron $0g_{9/2}$ orbital as well as a depletion of the proton $0f_{7/2}$ orbital. From table I, we also see an increase in the occupation number of the neutron $1d_{5/2}$ orbital for Ti, Cr, and Fe with respect to Ni. In other words, neutron excitations above the fp orbitals are favored for protons numbers below the 28 closed shell. This may be traced to a reduction of the neutron $0g_{9/2} - 0f_{5/2}$ gap as well as to the quadrupole-quadrupole component of the effective interaction acting between the $0g_{9/2}$ and $1d_{5/2}$ orbitals. The former argument is clearly evidenced in figure 4, where we report the behavior of the effective single-neutron energies as a function of Z.

C. ^{132}Sn neighboring

In the last ten years or so, nuclei in the mass region around ^{132}Sn have become accessible to experimental studies thanks to new RIB facilities and the development of sophisticate detection techniques. A large amount of experimental information has been acquired, but data for nuclei with $Z \sim 50$ and $N > 82$ still remain scarce. A further step in this direction will be certainly made with the next generation of RIB facilities. The available data

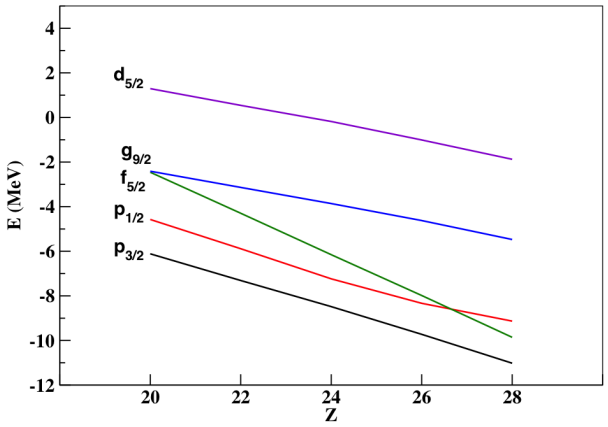

FIG. 4: (Color online) Calculated effective single-neutron energies for the $N = 40$ isotones.

for $N > 82$ nuclei have not evidenced changes in the shell structure, as it is was instead the case for the lighter nuclei discussed above. However, some anomalies have been observed. A notable one, which have posed interesting questions is, for instance, the asymmetric behavior with respect to $N = 82$ of the excitation energy of the yrast 2^+ state in both Sn and Te isotopes.

We have conducted several studies [21–24] on nuclei of this region, in all of them taking ^{132}Sn as closed core and assuming that proton particles and neutron holes occupy the five orbitals of the 50-82 shell, while neutron particles are in the six orbitals of the 82-126 shell. The single-particle and single-hole energies have been determined from experiment and the two-body effective interaction has been derived from the CD-Bonn NN potential renormalized by means of the $V_{\rm low-k}$ potential with $\Lambda = 2.2$ fm^{-1}. As for the calculation of the $\hat{Q}$-box, all diagrams up to second order have been taken into account, except the $(V - U)$-insertion diagrams which are limited to first order. All these studies, focused on energy spectra and electromagnetic properties, and more recently on spectroscopic factors and atomic masses, have led to results in very good agreement with experiment.

A main outcome of our work is that the pairing force plays a key role in determining the various properties of ^{132}Sn neighbors, as for instance the decrease in energy of the 2^+ state in ^{134}Sn and ^{136}Te. Our effective interaction, in fact, generates a pairing force between two neutrons in the 82-126 shell which is significantly weaker than that between two neutron holes or two proton particles in the 50-82 shell. Let us take, for instance, the $(\nu f_{7/2})^2$ configuration. The corresponding $J = 0^+$ matrix element is about -0.6 MeV to be compared to the value of -1 MeV or less for the $(\nu h_{11/2})^{-2}$ and $(\pi g_{7/2})^2$ configurations. This issue is discussed in [25], where we have investigated the origin of the pairing force within our microscopic framework and found that the above differences result from a large reduction of the core-polarization contributions to the neutron effective interaction for $N > 82$. It should be mentioned that the role of the pairing force in this mass region was also recognized in Refs.[26, 27].

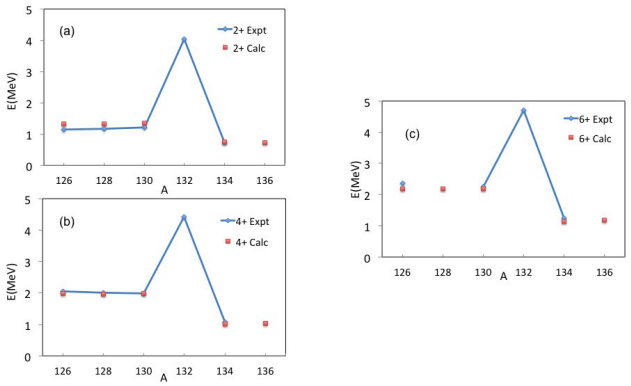

FIG. 5: (Color online) Calculated and experimental [15] excitation energies of the yrast (a) 2^+, (b) 4^+, and (c) 6^+ states in tin isotopes from $A = 126$ to 136.

To illustrate the quality of our results, we focus on the low-energy spectra and $B(E2)$ transition rates in Sn and Te isotopes. Then, as a final example, we discuss the odd-even staggering (OES) of binding energies for $N = 81$ and 83 isotones to show the predictive power of our approach in the calculation of binding energies.

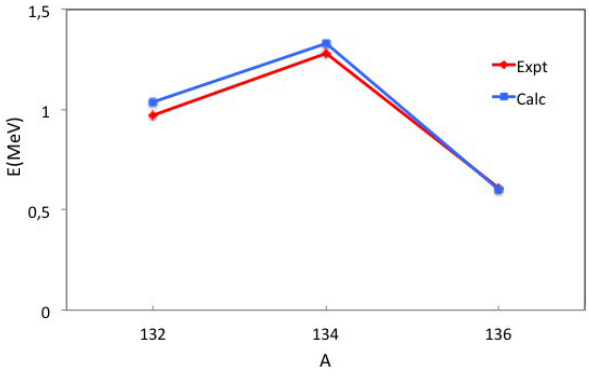

FIG. 6: (Color online) Calculated and experimental [15] excitation energies of the yrast 2^+ states in tellurium isotopes with $A = 132$, 134, and 136.

The theoretical and experimental excitation energies of the yrast 2^+, 4^+, and 6^+ states in Sn isotopes from $A = 126$ to 136 are compared in figure 5, while for Te isotopes we consider only the yrast 2^+ states for $A = 132$, 134, and 136, as shown in figure 6. We see that the available experimental data are very well reproduced by our calculation, including the marked decrease in the energies at $N = 84$. Note that for ^{136}Sn, for which no spectroscopic information is available, we predict a low energy spectrum quite similar to that of ^{134}Sn.

In table II the calculated $B(E2; 2_1^+ \rightarrow 0_1^+)$ transition rates, obtained with an effective proton and neu-

tron charge of 1.55 and $0.7e$, respectively, are compared with the experimental values. We see that in all cases, except for ^{136}Te, the agreement between theory and experiment is very good. More precisely, the discrepancy ranges between 12 and 22%, becoming larger than 50% in ^{136}Te. It is worth mentioning, however, that a new higher precision measurement of the $B(E2)$ in ^{136}Te is certainly needed, the present experimental value being determined from a reanalysis [23] of the experiment of Ref. [28]. At the same time, the predicted overestimation may be seen as an indication that our effective interaction lacks some accuracy. Actually, we pin down the main feature of the 2^+ state wave function, which turns out to be dominated by neutron excitations, but find that a 35% remaining weight is fragmented over various components, which are likely to lead to an enhancement of the B(E2).

TABLE II: Experimental [23, 29] and calculated $B(E2; 2_1^+ \rightarrow 0_1^+)$ (in W.u.) for Sn and Te isotopes .

	Expt	Calc
^{130}Sn	1.2(3)	1.4
^{134}Sn	1.4(2)	1.6
^{132}Te	10 (1)	7.8
^{134}Te	5.6 (6)	4.9
^{136}Te	5.9 (9)	9.9

As mentioned above, we conclude this section by discussing the neutron OES as defined by three-point formula

$$\Delta^{(3)}(N,Z) = \frac{1}{2}[B(N+1,Z) + B(N-1,Z) - 2B(N,Z)]. \quad (6)$$

By using our binding energies for ^{130,134}Sn, $^{132-136}$Te, and $^{134-138}$Xe, we have calculated the neutron OES for the $N = 81$ isotones ^{131}Sn, ^{133}Te, ^{135}Xe and for the $N = 83$ isotones ^{133}Sn, ^{135}Te, ^{137}Xe. They are compared with the experimental values in figure 7. We see that the agreement between theory and experiment is very good. In particular, our calculations give a quantitative description of the gap between the $N = 81$ and 83 lines at $Z = 50$ as well as of its decrease when adding two and four protons. The drop of about 0.5 MeV in the observed OES for Sn when crossing N= 82 is a consequence of the different pairing properties for neutron particles and holes with respect to the N= 82 closed shell. When going to Te and Xe, the $N = 81$ and 83 lines come closer to each other as a result of the proton-neutron effective interaction. The two lines would be indeed parallel should one ignore this interaction. From figure 7, we see that the *pn* interaction has an opposite effect on the $N = 81$ and $N = 83$ isotones, which is clearly related to its repulsive and attractive nature in the particle-hole and particle-particle channel, respectively. On the other hand, this effect is not very large either in ^{133,135}Te or in ^{135,137}Xe, since it results essentially from the difference between the contributions of the *pn* interaction to the energies of the odd and neighboring even isotopes.

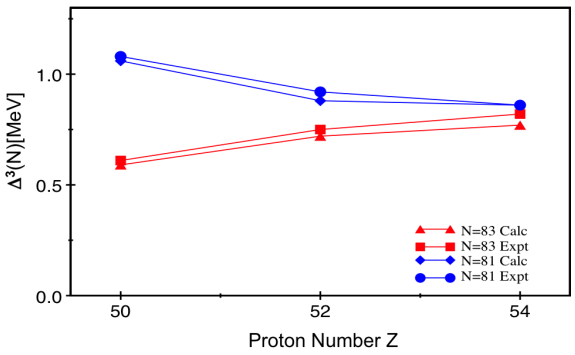

FIG. 7: (Color online) Calculated and experimental [30] odd-even staggering for the $N = 81$ and 83 isotones.

IV. SUMMARY AND CONCLUSIONS

In this paper, we have given a short overview of the shell-model approach with realistic effective interactions to the study of exotic nuclei. We have reviewed the main steps and the relevant recent developments involved in the derivation of these interactions and reported some selected results for neutron-rich nuclei in various mass regions, as oxygen isotopes, $N = 40$ isotones, and nuclei around ^{132}Sn. Actually, we have tried to give a panoramic view of our results, most of them already given in previous works, in order to illustrate the practical value of this approch as well as some of its limits.

The quality of our results has been highlighted in section 3 by comparison with the available experimental data. This shows that, with a few exceptions, observed spectroscopic properties as well as binding energies are well reproduced by the theory, proving the predictive power of realistic shell-model calculations. We have seen, however, that, when using theoretical single-particle energies, these calculations fail to reproduce the binding energies of the O isotopes. This may be traced to the lack of a three-body force, or more precisely to the contributions of this force to the one-body term of the effective Hamiltonian, while our results do not seem to evidence the need of an explicit three-body term or of renormalization of the two-body interaction.

Based on our calculations, we can conclude that nuclear structure results do not depend substantially on the choice of the free NN potential one starts with, when employing phase-shift equivalent low-momentum potentials. In this connection, we note that the effective interactions for the $N = 40$ isotones and ^{132}Sn neighbors are derived from the $V_{\rm low-k}$ of the CD-Bonn potentials with different cutoffs. We have also verified [31] that moderate

variations of the cutoff do not change significantly the shell-model results. However, further study is certainly needed on this point which has been examined essentialy for interactions derived at second order in the $\hat{Q}$-box.

The calculation of the $\hat{Q}$-box, as mentioned above, is one of the most critical point in our approach. Its convergenge properties are investigated in [9]. Here we point out that the quality of our results for nuclei around ^{132}Sn is very good when using a second-order $\hat{Q}$ box. One should consider, however, that calculations in this region are limited to nuclei near shell closures and cannot exclude that effects related to third order may appear for more valence neutrons (see comments in [11]). To conclude, we may say that realistic-shell model calculations represent by now a very effective tool to study nuclear structure. This makes it challenging to try to clarify some remaining open questions.

[1] Coraggio L, Covello A, Gargano A, Itaco N, Entem D R, Kuo T T S and Machleidt R 2007 *Phys. Rev.* C **75** 024311

[2] Coraggio L, Covello A, Gargano A, Itaco N and Kuo T T S 2011 *J. Phys. Conf. Ser.* **312** 092021

[3] Coraggio L, Covello A, Gargano A and Itaco N 2014 submitted to *Phys. Rev.* **C**

[4] Coraggio L, Covello A, Gargano A and Itaco N 2013 *Phys. Rev.* C **88** 041304(R) and references therein

[5] Machleidt R 2001 *Phys. Rev.* C **63** 024001

[6] Bogner S, Kuo T T S, Coraggio L, Covello A and Itaco N 2002 *Phys. Rev.* C **65** 051301(R)

[7] Ekström A, Baarsden G, Forssén, Hagen G, Hjorth-Jensen M, Jansen G R, Machleidt R, Nazarewicz W, Papenbrock T, Sarich J and Wild S M 2013 *Phys. Rev. Lett.* **110** 192502

[8] Coraggio L, Covello A, Gargano A, Itaco N and Kuo T T S 2009 *Prog. Part. Nucl. Phys.* **62** 135

[9] Coraggio L, Covello A, Gargano A, Itaco N and Kuo T T S 2012 *Ann. Phys.* **327** 2125

[10] Suzuki K and Lee S. Y. 1989 *Prog. Theor. Phys.* **64** 2091

[11] Covello A and Gargano A 2010 *J. Phys.* G **37** 064044

[12] Otsuka T, Suzuki T, Holt J D, Schwenk A, and Akaishi Y 2010 *Phys. Rev. Lett.* **105** 032501

[13] Hagen G, Hjorth-Jensen, M, Jansen G R, Machleidt R and Papenbrock T 2012 *Phys. Rev. Lett.* **108** 242501

[14] Hergert H, Binder S, Calci A, Langhammer J and Roth R 2013 *Phys. Rev. Lett.* **110** 242501

[15] Data extracted using the NNDC On-line Data Service from the ENSDF database, file revised as of January 8, 2014

[16] Wang M, Audi G, Wapstra A H, Kondev F G, MacCormick M, Xu X and Pfeiffer B 2012 *Chinese Phys.* C **36** 1603

[17] Lenzi S M, Nowacki F, Poves A and Sieja K 2010 *Phys. Rev.* C **82** 054301

[18] Rother W *et al.* 2011 *Phys. Rev. Lett.* **106** 022502

[19] Baugher T *et al.* 2012 *Phys. Rev.* C **86** 011305

[20] Crawford H L *et al.* 2013 *Phys. Rev. Lett.* **110** 242701

[21] Coraggio, L, Covello A, Gargano A and Itaco N 2009 *Phys. Rev* C **80** 021305(R) and references therein

[22] Covello A, Coraggio L, Gargano A and Itaco N 2011 *J. Phys. Conf. Ser.* **267** 01201 and references therein

[23] Danchev M *et al.* 2011 *Phys. Rev.* C **84** 061306(R)

[24] Coraggio L, Covello A, Gargano A and Itaco N 2013 *Phys. Rev.* C **87** 034309

[25] Covello A, Gargano A and Kuo T T S 2013 *Fifty Years of Nuclear BCS* ed R A Broglia and V Zelevinsky (Singapore: World Scientific) pp. 169-178

[26] Terasaki J, Engel J, Nazarewicz W and Stoitsov M 2002 *Phys. Rev.* C **66** 054313

[27] Shimizu N, Otsuka T, Mizusaki T and Honma M 2004 *Phys. Rev.* C **70** 054313

[28] Radford D C *et al.* 2002 *Phys. Rev. Lett.* **88** 222501

[29] Radford D C *et al.* 2005 *Nucl. Phys* A **752** 264c

[30] Hakala J. *et al.* 2012 *Phys. Rev. Lett.* **109** 032501

[31] Covello A, Coraggio L, Gargano A and Itaco N 2005 *J. Phys. Conf. Ser.* **20** 137